

Parafermions in a Kagome lattice of qubits for topological quantum computation

Adrian Hutter, James R. Wootton, and Daniel Loss

Department of Physics, University of Basel, Klingelbergstrasse 82, CH-4056 Basel, Switzerland

(Dated: May 7, 2015)

We show how \mathbb{Z}_4 parafermions emerge in a Kagome lattice composed of qubits with nearest neighbor two-qubit interactions. The low-energetic excitations of our model correspond to the Abelian $D(\mathbb{Z}_4)$ anyon model, and non-Abelian parafermion modes appear at the ends of defect lines. We prove that braiding of these parafermions with each other and with the $D(\mathbb{Z}_4)$ anyons allows us to generate the entire 4-level Clifford group. We study the error correction problem for our model in detail, guaranteeing fault-tolerance of the topological operations. Crucially, we do not need non-Abelian error correction but can correct the underlying Abelian model.

I. INTRODUCTION

Non-Abelian anyons enjoy a lot of interest due to the exciting physics they exhibit and due to their potential application for topological quantum computation [1–3]. The physical systems proposed to realize them, however, are often highly complex. The compatibility of these systems with the active error correction required for fault-tolerance is also rarely considered. Development of practical systems in which non-Abelian anyons may be created and manipulated is therefore required.

A particularly attractive approach for building a fault-tolerant quantum computer is to use a system of physical qubits (spin- $\frac{1}{2}$ particles). A number of technologies allow for precise qubit control, such as superconducting qubits [4], trapped atomic ions [5], spin qubits [6], or cold atoms or polar molecules in optical lattices [7]. A qubit lattice with two-body nearest neighbour interactions would therefore be an ideal system to realize non-Abelian anyons. It is thus important to find the most computationally powerful anyon model that can be realized on such a system, and which is compatible with quantum error correction.

Thus far, the only non-Abelian anyons known to be realized in qubit systems are Majorana zero modes, also known as Ising anyons. A variety of proposals for experimental realization of Majorana zero modes in solid state systems have also been developed [8]. They can be used to perform universal quantum computation when enhanced by non-topological operations [9, 10]. However, these additional operations are highly resource intensive. Anyon models with a richer set of topological operations would therefore be much more practical for the realization of topological quantum computation. One possibility is to use parafermion modes. These are generalizations of Majoranas with more complex and computationally powerful fusion and braiding behavior. This has led to a quest in recent years for systems that could host them. Numerous proposals for their experimental implementation in condensed matter systems such as fractional quantum Hall systems, nanowires, or topological insulators have recently appeared [11–22].

It is known how to engineer Majorana modes in qubit systems by using defect strings in $D(\mathbb{Z}_2)$ quantum dou-

ble models [23]. Parafermions, however, require $D(\mathbb{Z}_d)$ quantum double models which are based on higher dimensional systems [24]. The generalized Pauli operators appearing in these models coincide with the physically relevant spin-operators only for $d = 2$. Otherwise, their structure makes them highly difficult to realize experimentally. The case $d = 4$, however, allows us to combine the best of both worlds. The joint Hilbert space of two qubits allows the 4-dimensional generalized Pauli operators to be expressed in terms of two-qubit operators. Using this, we show how \mathbb{Z}_4 parafermions can emerge in a lattice of qubits with nearest-neighbor interactions only. This allows the computational power of \mathbb{Z}_4 parafermions to be harnessed in a qubit system.

The fact that our system is built on top of a system supporting Abelian anyons (the $D(\mathbb{Z}_4)$ quantum double model) proves very useful. The non-Abelian parafermion modes can not only be braided with each other, but also with Abelian excitations of the quantum double model, allowing us to generate the entire Clifford group by quasi-particle braiding. This extends beyond the limited set of gates found using the same parafermions in previous work [13]. Furthermore, we do not have to perform non-Abelian error correction (a still poorly understood problem [25–27]) to guarantee fault-tolerance, but can correct the underlying Abelian model. This Abelian error correction problem is nevertheless more involved than the well-studied error correction problem for the standard $D(\mathbb{Z}_d)$ models, and we study it in detail.

The rest of this paper is organized as follows. In Sec. II we show how \mathbb{Z}_4 parafermion operators can be expressed in terms of qubit operators. Sec. III introduces a qubit Hamiltonian whose low-energetic excitations correspond to the $D(\mathbb{Z}_4)$ quantum double model. In Sec. IV we discuss how \mathbb{Z}_4 parafermion modes appear at the ends of defect strings in our model. We demonstrate in Sec. V how the non-Abelian braiding statistics of these modes can be used to perform logical gates. Appendix D contains a proof that the set of gates which can be performed this way generates the entire Clifford group \mathcal{C}_4 , which may be of independent interest. In Sec. VI we study the error correction problem of our model in detail and conclude in Sec. VII.

II. \mathbb{Z}_4 PARA-FERMION OPERATORS IN TERMS OF QUBIT OPERATORS

We consider d -dimensional generalizations of the Pauli matrices X and Z . These are unitary operators satisfying $X^d = Z^d = \mathbb{1}$ and $ZX = \omega XZ$, where $\omega = e^{2\pi i/d}$ with integer $d > 1$. If we define $Y = X^\dagger Z^\dagger$ it follows that $XYZ = \mathbb{1}$ and $Y^d = \omega^{d(d-1)/2} \mathbb{1}$. Operators X_i and Z_i act on qudit i and hence $[X_i, X_j] = [Z_i, Z_j] = [X_i, Z_j] = 0$ if $i \neq j$.

These operators are related to those of parafermions. Given a total ordering on the qudits $\{i\}$, one can obtain parafermion operators via a non-local transformation [28]

$$\gamma_{2i-1} = \left(\prod_{j < i} X_j\right) Z_i, \quad \gamma_{2i} = \omega^{(d+1)/2} \left(\prod_{j \leq i} X_j\right) Z_i. \quad (1)$$

These satisfy the \mathbb{Z}_d parafermion relations,

$$\gamma_j^d = \mathbb{1}, \quad \gamma_j \gamma_k = \omega^{\text{sgn}(k-j)} \gamma_k \gamma_j. \quad (2)$$

The operators X , Y , and Z can be represented as d -dimensional matrices. It is thus natural to seek a representation of these operators for the case $d = 4$ on the Hilbert space of two qubits (spins- $\frac{1}{2}$). Indeed, given two qubits 1 and 2, one easily verifies that the operators

$$\begin{aligned} X &= \frac{1}{2} \sigma_1^x + \frac{1}{2} \sigma_2^x - \frac{i}{2} \sigma_1^z \sigma_2^y + \frac{i}{2} \sigma_1^y \sigma_2^z \\ Y &= -\frac{i}{2} \sigma_1^y + \frac{1}{2} \sigma_2^y + \frac{1}{2} \sigma_1^x \sigma_2^z - \frac{i}{2} \sigma_1^z \sigma_2^x \\ Z &= \frac{1+i}{2} \sigma_1^z + \frac{1-i}{2} \sigma_2^z \end{aligned} \quad (3)$$

are 4-dimensional generalized Pauli operators, and \mathbb{Z}_4 parafermions can be obtained from these via Eq. (1). We also note that $X^2 = \sigma_1^x \sigma_2^x$, $Y^2 = -i \sigma_1^y \sigma_2^y$, and $Z^2 = \sigma_1^z \sigma_2^z$.

III. MODEL

We consider a two-dimensional Kagome (trihexagonal) lattice as in Fig. 1. Each vertex of the lattice hosts one 4-dimensional qudit (one pair of \mathbb{Z}_4 parafermions) or, in other words, two qubits. The Hamiltonian of our model is given by

$$H = \sum_{\Delta} H_{\Delta} + h \sum_i (\sigma_{i1}^x + \sigma_{i2}^x). \quad (4)$$

Here, the first term is a sum of equivalent terms for each triangle in the Kagome lattice. We label the vertices around one triangle a , b , and c , and the two qubits which are present at vertex a are called a_1 and a_2 , etc. The triangle terms in the Hamiltonian are then given by

$$\begin{aligned} H_{\Delta} &= \frac{J}{2} (\sigma_{a1}^z \sigma_{b1}^z \sigma_{c1}^z + \sigma_{a2}^z \sigma_{b2}^z \sigma_{c2}^z) \\ &\quad - \frac{J}{2} (\sigma_{a1}^z \sigma_{b1}^z \sigma_{c2}^z + \sigma_{a1}^z \sigma_{b2}^z \sigma_{c1}^z + \sigma_{a2}^z \sigma_{b1}^z \sigma_{c1}^z \\ &\quad + \sigma_{a2}^z \sigma_{b2}^z \sigma_{c1}^z + \sigma_{a2}^z \sigma_{b1}^z \sigma_{c2}^z + \sigma_{a1}^z \sigma_{b2}^z \sigma_{c2}^z). \end{aligned} \quad (5)$$

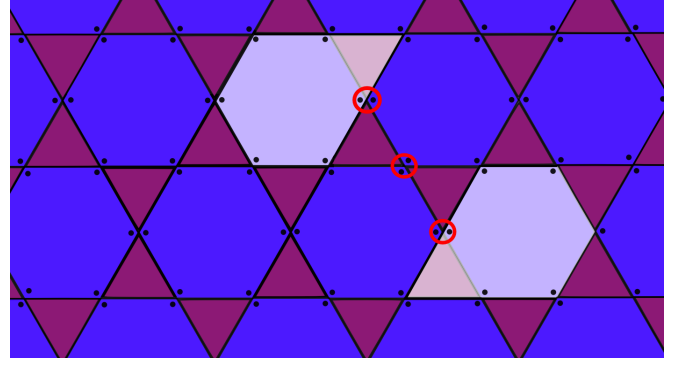


FIG. 1. Two qubits are located at each vertex of a Kagome lattice. Each pair of qubits hosts two \mathbb{Z}_4 parafermions. To unlock their potential for non-Abelian braiding, two such parafermions need to become unpaired, which is achieved by adding a defect line to the lattice. These are strings of strong local operators acting on qubit pairs (encircled). They create unpaired parafermion modes located at their ends (light pentagon-shaped regions consisting of a hexagon and a triangle).

The second sum \sum_i in Eq. (4) runs over all vertices in the lattice. The two qubits located at vertex i are called $i1$ and $i2$. This second sum thus represents a uniform magnetic field in x -direction.

Our Hamiltonian involves three-qubit terms of the form $\sigma_a^z \sigma_b^z \sigma_c^z$. It is in principle straightforward to generate these from one-body terms and two-body interactions by use of perturbative gadgets [29–31]. Consider a “mediator qubit” u coupled to qubits a , b , and c . Starting from a Hamiltonian

$$H_{\text{gadget}} = -\frac{\Delta}{2} \sigma_u^z + \alpha (\sigma_a^z + \sigma_b^z) \sigma_u^x + \beta \sigma_c^z \sigma_u^z + \gamma \sigma_a^z \sigma_b^z + \delta \sigma_c^z, \quad (6)$$

and consider the perturbative regime $\Delta \gg |\alpha|, |\beta|$. In this regime, it is possible to integrate out qubit u . Taking up to third-order terms into account, one finds an effective Hamiltonian

$$H_{\text{eff}} = (\beta + \delta) \sigma_c^z + (-2 \frac{\alpha^2}{\Delta} + \gamma) \sigma_a^z \sigma_b^z - 4 \frac{\alpha^2 \beta}{\Delta^2} \sigma_a^z \sigma_b^z \sigma_c^z. \quad (7)$$

Choosing $\delta = -\beta$ and $\gamma = 2 \frac{\alpha^2}{\Delta}$ produces the desired three-qubit term without any undesired one- or two-qubit terms.

The generation of three-body interactions in optical lattices has been discussed in detail in Refs. [32, 33]. These proposals would make the perturbative gadgets unnecessary. A “toolbox” for generating spin-lattice models such as ours in optical lattices has also been developed [34].

The spin-Hamiltonian in Eq. (4) can be exactly rewritten as

$$H = -J \sum_{\Delta} (Z_a Z_b Z_c + \text{H.c.}) + h \sum_i (X_i + X_i^\dagger). \quad (8)$$

Here again the first sum runs over all triangles in the lattice and the corners of a triangle are labeled a , b , and c . The second sum runs again over all vertices of the lattice.

We now consider the perturbative limit $h \ll J$ and regard the second sum in Eq. (8) as a perturbation to the first term. Note that all terms in the first sum in Eq. (8) commute, so the unperturbed Hamiltonian is trivially solved. The lowest-order non-vanishing terms appear in sixth-order perturbation theory. We find an effective Hamiltonian

$$H_{\text{eff}} = -J \sum_{\triangle} (Z_a Z_b Z_c + \text{H.c.}) - \frac{63}{8} \frac{h^6}{(2J)^5} \sum_{\hexagon} (X_r X_s^\dagger X_t X_u^\dagger X_v X_w^\dagger + \text{H.c.}), \quad (9)$$

where the second sum runs over all hexagons in the Kagome lattice and r, s, t, u, v, w label the six vertices around each hexagon. The effective Hamiltonian in Eq. (9) is derived in Appendix A.

We note that all summands in H_{eff} commute, so the system is exactly solvable. The excitations of this system are Abelian anyons corresponding to the $D(\mathbb{Z}_4)$ quantum double model. The topological degeneracy of the model can be made manifest by studying non-local loop degrees of freedom that commute with all stabilizers $Z_a Z_b Z_c$, $X_r X_s^\dagger X_t X_u^\dagger X_v X_w^\dagger$, and their Hermitian conjugates, and fulfill themselves \mathbb{Z}_4 relations. A possible choice of operators is illustrated in Fig. 2.

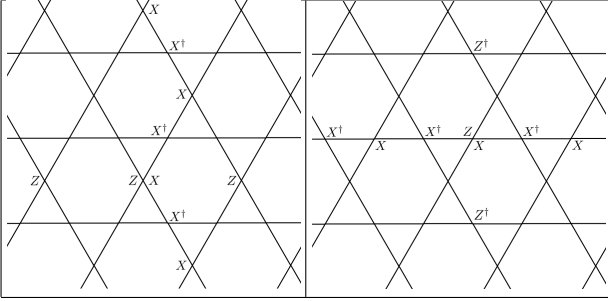


FIG. 2. Two sets of logical operators $\tilde{X}_1 = XX^\dagger XX^\dagger \dots$, $\tilde{Z}_1 = ZZZZ \dots$ (left figure) and $\tilde{X}_2 = XX^\dagger XX^\dagger \dots$, $\tilde{Z}_2 = ZZ^\dagger ZZ^\dagger \dots$ (right figure) that satisfy the commutation relations of 4-dimensional generalized Pauli operators.

In passing, we note that the \mathbb{Z}_2 version of Eq. (8), in which the \mathbb{Z}_4 operators X and Z are replaced by Pauli operators σ^x and σ^z , leads to an effective Hamiltonian analogous to Eq. (9) and thus provides a very simple model with topological order. While this model requires three-body operators $\sigma^z \sigma^z \sigma^z$ as opposed to Kitaev's honeycomb Hamiltonian [35] which involves two-body interactions only, all of these interactions connect the same spin-component, which may provide a significant practical simplification over the honeycomb model.

IV. PARA-FERMION MODES AND DEFECT LINES

The model is constructed from the cyclic qudit operators Z and X , which are related to parafermion operators. It is therefore natural to seek an interpretation of the model in terms of parafermionic modes.

To do this we must first fix the exact form of the stabilizers, which define the anyonic charge carried by each excitation. Let us use E_p (M_p) to denote the stabilizer for a hexagonal (triangular) plaquette, p . For hexagonal plaquettes we use the convention that $E_p = X_r X_s^\dagger X_t X_u^\dagger X_v X_w^\dagger$, where r refers to the top-right corner and the other corners are labelled in an anti-clockwise fashion. For triangular plaquettes we use $M_p = Z_a Z_b Z_c$ for all triangles of the form \triangle and $M_p = Z_a^\dagger Z_b^\dagger Z_c^\dagger$ for all triangles of the form ∇ . The stabilizer operators E_p and M_p are unitary operators with eigenvalues ω^k , $k \in \{0, 1, 2, 3\}$, where here and in the following $\omega = i$ for $d = 4$. An eigenvalue ω^g of the E_P corresponds to a charge anyon of the form e_g , while M_P similarly detects flux anyons m_h . Fusion of charge anyons forms a representation of \mathbb{Z}_4 , as does that of fluxes. The convention for the stabilizer operators chosen before ensures that the anyonic charge of both charge and flux type anyons is independently conserved (modulo 4). A full clockwise monodromy of an e_g around an m_h , or *vice versa*, yields a phase ω^{gh} .

Just as Majorana modes (Ising anyons) in the qubit toric code [23, 24], parafermions appear in our system at the ends of defect strings. For the interpretation in terms of parafermions, it will be useful to introduce a new set of composite anyons defined as $\psi_g = e_g \times m_g$. These also obey \mathbb{Z}_4 fusion with each other, and their braiding behavior can be inferred from the behavior of the constituent charge and flux particles. The particles $\{\psi_0, \psi_1, \psi_2, \psi_3\}$ form a chiral Abelian anyon model with Chern number $\nu = 2$ [35].

Note that

$$e_g \times m_h = \psi_g \times m_{h-g}. \quad (10)$$

We now perform a local transformation from the set of stabilizer generators $\{E_p, M_p\}$, detecting the charges on the left-hand-side of Eq. (10), to a new set $\{S_p, R_p\}$ which detects the two charges on the right-hand-side. Let H denote the set of hexagonal plaquettes and T denote the set of triangular plaquettes. Note that $|T| = 2|H|$. Consider an injective map $\varphi : H \rightarrow T$, which to each hexagonal operator E_p assigns one of the six adjacent triangular operators $M_{\varphi(p)}$. Typically, we choose $M_{\varphi(p)}$ to be the top-right neighbor of E_p , while other choices become necessary next to defect lines. The transformation from the old to the new set of stabilizers reads $S_p = E_p$ for $p \in H$ and

$$R_p = \begin{cases} M_p E_{\varphi^{-1}(p)}^\dagger & \text{if } p \in \text{Im}(\varphi) \\ M_p & \text{if } p \notin \text{Im}(\varphi) \end{cases} \quad (11)$$

for $p \in T$.

Since $\prod_{p \in H} S_p = \prod_{p \in T} R_p = \mathbb{1}$, the charges detected by the new stabilizers are separately conserved (modulo 4). Just like the ψ_g anyons detected by the S_p stabilizers, the R_g charges detected by the R_p stabilizers also form an anyon model obeying \mathbb{Z}_4 fusion. However, while these two anyon models have the same fusion rules, they are not equivalent, as they exhibit different braiding behavior. A full clockwise monodromy of a ψ_g around a ψ_h gives a phase of ω^{2gh} , a monodromy of a r_g around an r_h gives a phase of 1, and a monodromy of a ψ_g around a r_h gives a phase of ω^{gh} . Just like the e_g and m_h charges, the ψ_g and r_h particles correspond to a way of decomposing the $D(\mathbb{Z}_4)$ model into two submodels which are closed under fusion, but have non-trivial mutual braiding behavior,

$$\begin{aligned} D(\mathbb{Z}_4) &= \{e_0, e_1, e_2, e_3\} \times \{m_0, m_1, m_2, m_3\} \\ &= \{\psi_0, \psi_1, \psi_2, \psi_3\} \times \{r_0, r_1, r_2, r_3\}, \end{aligned} \quad (12)$$

where the three particle models other than $\{\psi_0, \psi_1, \psi_2, \psi_3\}$ correspond to the simple \mathbb{Z}_4 model.

The stabilizer operators S_p detect the presence of ψ_g anyon which are pinned to a pentagon-shaped double plaquette, made up of a neighbouring pair of triangular and hexagonal plaquettes. These anyons can be regarded as generalizations of Dirac fermions to the group \mathbb{Z}_4 (rather than \mathbb{Z}_2). Just as Dirac modes can be decomposed into two Majorana modes, so too can the ψ modes be decomposed into two parafermion modes. Two parafermion modes, P_a and P_b , are therefore associated with each double plaquette, P . These are described using parafermion operators satisfying Eq. (2). The parity operator for the ψ mode associated with a pair (j, k) is defined $\omega^{3/2} \gamma_j \gamma_k^\dagger$, and so $S_P = \omega^{3/2} \gamma_{P_a} \gamma_{P_b}^\dagger$.

For a stabilizer state, the system is within a definite eigenstate of all S_P . The parafermion modes are therefore all paired, with the pairs corresponding to the two within each double plaquette. In order to use the parafermion modes as non-Abelian anyons, some must be allowed to become unpaired. The creation and transport of unpaired parafermion modes can be done by adapting the method of Ref. [24] to the Kagome lattice. The method can be interpreted in terms of anyonic state teleportation [36], as explained for the Majorana case in Ref. [37].

The method introduces unpaired parafermion modes at the endpoints of defect lines. These are lines on which additional single qudit terms are added to the Hamiltonian, of one of the two following forms

$$\begin{aligned} \omega^{3/2} Y_i + \text{H.c.} &= \frac{1}{\sqrt{2}} (\sigma_1^y - \sigma_2^y - \sigma_1^x \sigma_2^z + \sigma_1^z \sigma_2^x), \\ \omega^{3/2} X_i Z_i^\dagger + \text{H.c.} &= \frac{1}{\sqrt{2}} (\sigma_1^y + \sigma_2^y - \sigma_1^x \sigma_2^z - \sigma_1^z \sigma_2^x). \end{aligned} \quad (13)$$

Specific examples are shown in Fig. 3.

The single qudit terms added along defect lines are much stronger than any other interactions, and thus effectively remove the qudits on which they act from the

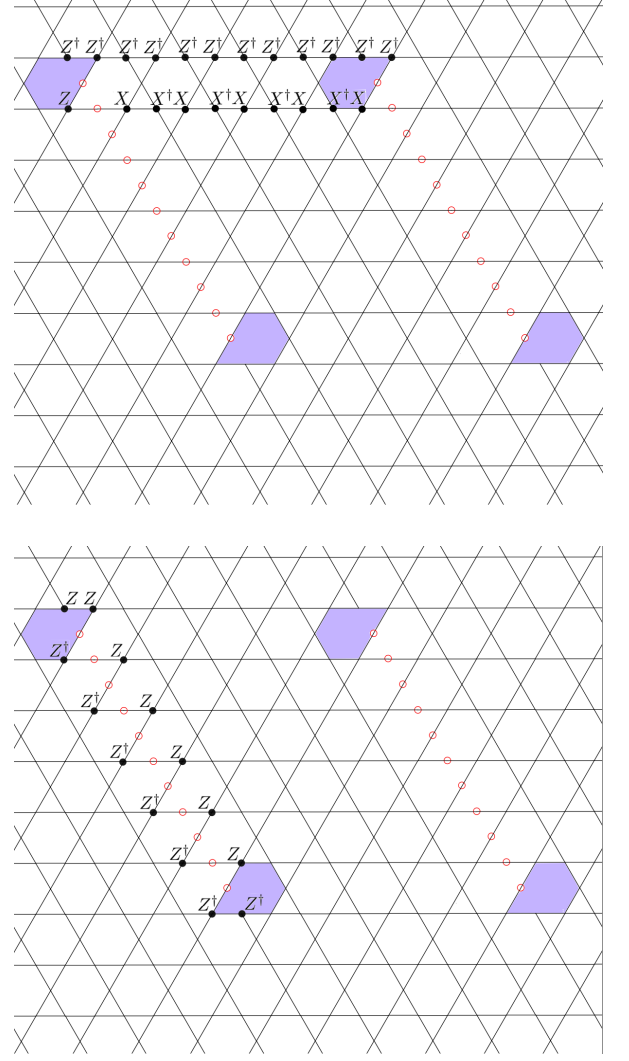


FIG. 3. Strings of alternating single-qudit operators of the form $\omega^{3/2} Y_i + \text{H.c.}$ or $\omega^{3/2} X_i Z_i^\dagger + \text{H.c.}$ (encircled) are added to the Hamiltonian. These effectively eliminate the qudits on which they act from the code, leading to enlarged, pentagon-shaped stabilizers along the defect string. Parafermion modes reside on the pentagons at the ends of the defect strings (shaded). A possible choice for two logical operators \tilde{X}_L (top) and \tilde{Z}_L (bottom) satisfying $\tilde{Z}_L \tilde{X}_L = \omega \tilde{X}_L \tilde{Z}_L$ is illustrated.

code. This means that the E_P and M_P operators for the double plaquettes along these lines no longer commute with the Hamiltonian, and so can no longer be used as stabilizer generators. Their pentagon-shaped product, R_P , is used instead. The pentagons in Fig. 3 show how next to a defect line the mapping φ needs to pick the bottom-left triangular-shaped stabilizer of a hexagon-shaped stabilizer to ensure that their product still commutes with the Hamiltonian.

This change of the stabilizer generators of the code has a drastic effect. Consider an e_g anyon moved towards a point along a defect line from one direction, and an m_g

moved towards the same point from the other direction. Both of these are detected by R_P type stabilizers. When they meet on the same double plaquette, they will fuse to form a ψ_g , and so not be detected by the R_P stabilizers anymore. In fact, since the S_P stabilizer is removed for double plaquettes along a defect line, they will not be detected by any stabilizer operator. The ψ_g occupancy of a defect line corresponds to an increased groundstate degeneracy of the system, referred to as a *synthetic topological degeneracy* [24].

In the following section, the $\{\psi_g, w_h\}$ decomposition of the $D(\mathbb{Z}_4)$ model will prove more convenient than the $\{e_g, m_h\}$ decomposition. A process in which a defect line converts an m_g into an e_{-g} can equivalently be described as one in which a r_g passes a defect line which emits a ψ_{-g} .

V. PARA-FERMIONS AS NON-ABELIAN ANYONS

Since unpaired parafermion modes reside at the endpoints of defect strings, it is natural to use them to explain the properties of the modified stabilizer. Parafermion modes are described by a non-Abelian anyon model with particle species $\{\psi_0, \psi_1, \psi_2, \psi_3, \sigma\}$. Here $\psi_0 \equiv 1$ corresponds to the anyonic vacuum and σ is an unpaired parafermion mode. The fusion rules of this anyon model are

$$\begin{aligned} \sigma \times \sigma &= \psi_0 + \psi_1 + \psi_2 + \psi_3, \\ \psi_g \times \psi_h &= \psi_{g \oplus h}, \\ \psi_g \times \sigma &= \sigma, \end{aligned} \quad (14)$$

where \oplus denotes addition modulo 4. A pair of parafermions (or the defect line between them) may therefore collectively hold any of the four types of ψ anyon.

As in the Majorana/Ising case, we use four parafermion modes (two defect strings) for which the total fusion sector is vacuum to store one logical qudit. The natural logical operators are parity operators for the pairs of parafermions. An eigenvalue ω^g corresponds to a ψ_g occupancy for the pair, and so the specific result $\sigma \times \sigma = \psi_g$ if they would be fused. We associate the Z basis of the logical qudit with the ψ occupancy of vertical pairs (connected by defect lines).

Specific choices of logical operator are illustrated in Fig. 3. The \tilde{Z}_L corresponds to a clockwise loop of an e_1 around a defect line. The braiding of this e_1 around the ψ_g held in the pair yields the required phase of ω^g . The \tilde{X}_L corresponds to clockwise loop of an e_{-1} anyon which is converted to an m_1 through one defect line and back to an e_{-1} through the other. Equivalently, we can describe it as a clockwise loop of a w_1 and a transfer of a ψ_1 from the right to the left defect line.

Let us denote a state in which the left defect line holds a mode ψ_g and the right defect line holds a mode ψ_h by

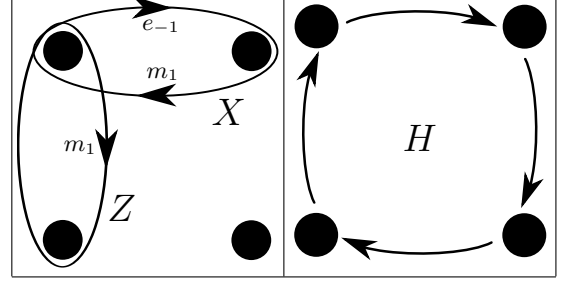


FIG. 4. All generators of the single-qudit Clifford group can be performed by braiding quasi-particles. The four circles correspond to the four parafermion modes which are used to store one logical qudit. The left part of the figure illustrates how to perform the logical operators X and Z by braiding the Abelian excitations of the $D(\mathbb{Z}_4)$ model around the parafermions. The right part demonstrates a logical Hadamard gate H , which is performed by braiding the parafermion modes themselves.

$|\psi_g, \psi_h\rangle$. Two defect lines create a 4×4 -fold synthetic topological degeneracy. For computational purposes, we restrict to the 4-dimensional subspace of states of the form $|g\rangle_L \equiv |\psi_g, \psi_{-g}\rangle$. This is the set of states which can locally be created from the anyonic vacuum. The effect of the logical operators on these states is $\tilde{X}_L |g\rangle_L = |g \oplus 1\rangle_L$ and $\tilde{Z}_L |g\rangle_L = \omega^g |g\rangle_L$.

In addition to the logical operators \tilde{X}_L and \tilde{Z}_L , which can be performed in our model by braiding the Abelian $D(\mathbb{Z}_4)$ anyons around the parafermion modes (ends of defect strings), we can perform further topologically protected single-qudit and two-qudit gates by braiding the parafermion modes themselves. Defect lines used for braiding are shown in Appendix B. Crucially, braiding parafermions allows one to perform an entangling gate by topological means, which is in contrast to Majorana fermions [13]. What is more, exploiting the fact that our non-Abelian system is built on top of an Abelian $D(\mathbb{Z}_4)$ system allows us to generate the entire 4-level Clifford group by braiding quasi-particles, as we discuss in the following.

For the rest of this section, X and Z refer to the logical operators called \tilde{X}_L and \tilde{Z}_L before, respectively. The first column in Fig. 4 illustrates how braiding of $D(\mathbb{Z}_4)$ charges and fluxes can be used to perform logical X and Z gates. Whether an e_1 or an m_1 anyon is used to perform the logical Z gate is irrelevant.

Consider two parafermion modes storing a ψ_g particle. A full clockwise monodromy of one parafermion around the other can be understood as a monodromy of the constituent e_g around the m_g , yielding an ω^{g^2} phase. Likewise, a clockwise exchange of the two parafermion modes storing a ψ_g yields a phase $\omega^{g^2/2}$, as we demonstrate directly by studying the necessary microscopic operations in App. C.

For a logical qudit stored in four parafermion modes,

let S denote a clockwise exchange of a vertical pair of parafermion modes, and T an exchange of a horizontal pair. As discussed, we have $S|g\rangle_L = \omega^{g^2/2}|g\rangle_L$, while T is diagonal in the logical X basis. In the logical Z basis, the matrix elements of T are given by

$$\langle g|_L T |h\rangle_L = \begin{cases} (-1)^{(g-h)/2} \frac{\sqrt{2}}{4} (1+i) & \text{if } g = h \pmod{2} \\ \frac{1}{2} & \text{if } g \neq h \pmod{2} \end{cases}. \quad (15)$$

Again, in contrast to Majorana fermions, parafermions support an entangling gate between two logical qudits by braiding operations [13]. The controlled phase-gate Λ is defined by its action on a two-qudit basis state, $\Lambda|g, h\rangle_L = \omega^{gh}|g, h\rangle_L$. In our parafermion scheme, an entangling gate can be performed by braiding of a pair of parafermions from one qudit with a pair from the other. Let us consider, for example, the braiding of the left vertical pair for both qudits. For an initial state $|g, h\rangle_L$, the process corresponds to braiding a ψ_g clockwise around a ψ_h , which yields a phase of ω^{2gh} . The resulting operation is therefore the squared controlled phase-gate Λ^2 . For $d = 2$, corresponding to the Ising/Majorana case, $\Lambda^2 = \mathbb{1}$, and so this operation is trivial. For $d > 2$, however, it is a non-trivial entangling gate, akin to the one proposed in Ref. [13].

Clearly a more powerful entangling gate would be Λ itself. This can be achieved for \mathbb{Z}_d parafermions for odd d by taking the $(d+1)/2$ -th power of Λ^2 . However these do not admit the simple decomposition into qubits that we have used in defining the model. Fortunately, we can make use of the underlying charge and flux anyons to realize Λ despite the even qudit dimension.

The defect line may be interpreted as a hole for ψ type anyons: an area in which they may be placed such that their state becomes delocalized along the line and they are no longer detected by the stabilizers [39, 40]. Similar holes can also be engineered for the constituent charge and flux anyons. A defect line is therefore a special case of the combination of a charge and flux hole, in which only $\psi_g = e_g \times m_g$ type anyons may reside rather than general $e_g \times m_h$ anyons. Nevertheless, we can consider a process in which a defect line is transformed into a separate charge and flux hole. When only the charge hole of one qudit is braided around the defect line of another, the process for an initial state $|g, h\rangle_L$ corresponds to braiding an e_g around a ψ_h , which would yield the phase ω^{gh} . The charge and flux holes can then be recombined into a defect line. The net effect of the entire process is to apply the controlled phase gate Λ . Such a process is illustrated in Fig. 5.

One process which could split the defect line in this way is simply to intersect it with two others. One would be a line along which charge anyons are hopped by high-strength terms. The other would similarly hop flux anyons. The stabilizers that detect charges and fluxes, respectively, along these lines would then be suppressed. By adiabatically removing the defect line which delocal-

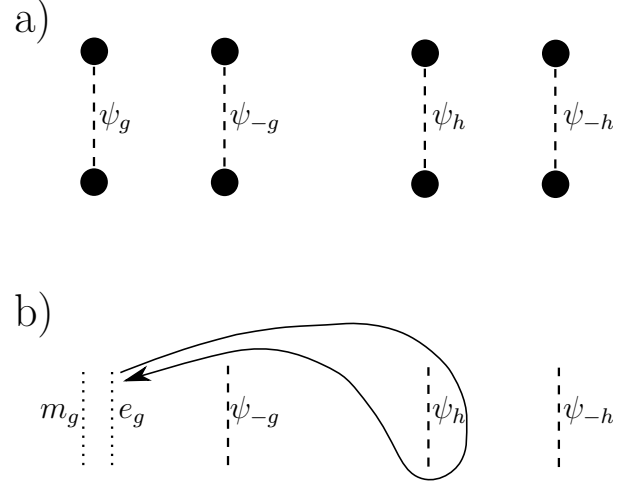


FIG. 5. Performance of a controlled phase-gate. The a) part of the figure shows a logical product state $|g, h\rangle_L$ stored in the fusion space of eight parafermions. The defect line storing a mode ψ_g can be split into two defect lines storing $D(\mathbb{Z}_4)$ charges e_g and m_g , respectively. Braiding both endpoints of one of these lines clockwise around the defect line storing the ψ_h mode, as shown in the b) part, produces a phase ω^{gh} , as required.

izes ψ modes, its ψ_g anyon occupation would be transferred to these two lines. The recombination of the defect line would be done by the reverse process.

For a tensor product of d -level systems, the Clifford group \mathcal{C}_d consists of gates that map tensor products of d -level Pauli operators to other such tensor products under conjugation. In Appendix D, we prove the following theorem.

Theorem. *The single-qudit gates S , T , and Z , and nearest-neighbor controlled phase-gates Λ generate the entire Clifford group \mathcal{C}_4 .*

As an example, $\tilde{H} = STS = TST$ satisfies $\tilde{H}X\tilde{H}^\dagger = Z$ and $\tilde{H}Z\tilde{H}^\dagger = X^\dagger$, so it can be identified with the logical Hadamard gate, up to a phase. Indeed, using the standard definition

$$H = \frac{1}{\sqrt{d}} \sum_{gh} \omega^{gh} |g\rangle \langle h|, \quad (16)$$

one verifies that $\sqrt{\omega}H = \tilde{H}$.

One possible implementation of H (up to a phase) is a cyclic permutation of the four parafermion modes, as in Fig. 4. This can be pictorially understood as follows. An X corresponds to a transfer of a ψ_1 from the right to the left defect line, accompanied by a clockwise loop of a r_1 around a horizontal pair. A Z corresponds to a clockwise loop of a r_1 around a vertical pair. A $\pi/2$ rotation as performed by H thus maps these two operations onto each other, up to the fact that we do not perform a vertical ψ_1 transfer, as the ψ occupancy of the vertical

pair is delocalized along the defect line.

VI. ERROR CORRECTION

For any system with a finite energy gap at finite temperature, excitations will appear with a finite density. This corresponds to finite length scale on which quantum computation can be performed before errors are almost certain to appear. This length scale can be increased by increasing the gap or lowering the temperature. However, neither of these methods is truly scalable. Error correction is therefore required if scalable quantum computation is to be performed.

For non-Abelian systems, the first studies of the corresponding error correction problem have recently appeared [25–27]. Error correction for non-Abelian anyons is still poorly understood and its feasibility has not been demonstrated for the (realistic) time-continuous case. It comes thus very welcome that while our system provides the computational power of non-Abelian parafermions, its physical excitations still are Abelian $D(\mathbb{Z}_4)$ anyons, and the error correction problem for $D(\mathbb{Z}_n)$ quantum double models (including the time-continuous case) is well-studied [27, 41–43]. However, when correcting these $D(\mathbb{Z}_4)$ anyons, we face a number of difficulties not considered in previous studies [27, 41–43]:

- (i) Our stabilizer operators are products of \mathbb{Z}_4 qudit operators X , X^\dagger , Z , Z^\dagger , while an error model is realistically expressed in terms of single-qubit operators σ^x , σ^y , σ^z . These do not map eigenstates of the stabilizer operators to other eigenstates and one single-qubit operator can produce a product of up to three qudit operators (see below).
- (ii) We consider quantum information stored in a synthetic topological degeneracy, which involves a defect line allowing anyons to change from one sublattice to the other (stars to hexagons and *vice versa*). We thus cannot decode each sublattice separately, as usually done for the toric code and other $D(\mathbb{Z}_d)$ quantum double models, but have to correct both of them simultaneously while taking the possibility of transferring anyons from one to the other into account.
- (iii) Besides simplistic i.i.d. error models (such as depolarizing noise), we are particularly interested in Hamiltonian protection of a quantum state subject to thermal errors.
- (iv) We do not consider a quadratic lattice, but a trihexagonal one, which makes moving anyons and defining their distance more involved.

σ_1^x, σ_2^x	$X, X^\dagger, XZ^2, X^\dagger Z^2$
σ_1^y, σ_2^y	$XZ, X^\dagger Z, XZ^\dagger, X^\dagger Z^\dagger$
σ_1^z, σ_2^z	Z, Z^\dagger

TABLE I. Conversion from single-qubit Pauli operators to 4-dimensional generalized Pauli operators. When a syndrome measurement is performed, a Pauli operator is converted to each of the generalized Pauli operators in the right-hand column with equal probability.

A. Error model

Since our 4-level qudits are composed of two qubits, it is natural to consider an error model in terms of single-qubit operations σ^x , σ^y , and σ^z . For a qudit hosted in two qubits 1 and 2, single-qubit Pauli operators can be expressed in terms of \mathbb{Z}_4 operators by inverting Eq. 3. We find

$$\begin{aligned}\sigma_1^x &= \frac{1}{2}X(1 - Z^2) + \text{H.c.}, & \sigma_2^x &= \frac{1}{2}X(1 + Z^2) + \text{H.c.}, \\ \sigma_1^y &= \frac{i}{2}Y(1 + Z^2) + \text{H.c.}, & \sigma_2^y &= \frac{1}{2}Y(1 - Z^2) + \text{H.c.}, \\ \sigma_1^z &= \frac{1-i}{2}Z + \text{H.c.}, & \sigma_2^z &= \frac{1+i}{2}Z + \text{H.c.}\end{aligned}\quad (17)$$

If we start from an eigenstate of all stabilizer operators, applying single-qubit Pauli operators will generate a superposition of states corresponding to different syndrome outcomes. By measuring all stabilizer operators, we can project again into a subspace with definite syndrome values. Each single-qubit Pauli operator thereby translates into a product of up to three qudit operators. Table I summarizes (up to irrelevant phases) into which qudit operators a certain single-qubit Pauli operator will translate with equal probability.

As a first simple error model, which does not involve a notion of Hamiltonian protection, we consider depolarizing noise. That is, for each qubit of the code we apply a Pauli operator with some probability p (the *depolarization rate*), where each of the three Pauli operators is chosen with equal probability.

More interesting from a physical perspective is a thermal error model. We consider a quantum state stored in the degenerate groundstates of the Hamiltonian given in Eq. (9), and assume that the system is weakly coupled to a heat bath at some temperature T . Following e.g. Ref. [26], we assume that evolving the system according to the Metropolis algorithm provides a reasonable approximation of the thermalization process, since the evolution obtained by means of the Metropolis algorithm is local, Markovian, and has the thermal state as its unique fixed point.

During our simulation, we proceed as follows. We first pick one of the spins- $\frac{1}{2}$ of the system at random, then pick one of the three single-qubit operators acting on that qubit at random, and convert that to a 4-dimensional generalized Pauli operator according to Table I. We then

calculate the energy cost Δ_{tot} of applying that generalized Pauli operator (or products thereof). This energy cost is of the form

$$\Delta_{\text{tot}} = m\Delta_{\Delta} + n\Delta_{\square}, \quad (18)$$

where Δ_{Δ} and Δ_{\square} are the energy costs of creating a single triangle/hexagon-type anyon with charge 1 or 3 in Eq. (9), respectively. (That is, $\Delta_{\Delta} = 2J$ and $\Delta_{\square} = 2\frac{63}{8}\frac{h^6}{(2J)^5}$.) Creating an anyon with charge 2 will have an energy cost $2\Delta_{\Delta}$ or $2\Delta_{\square}$. The coefficients m and n are elements of $\{0, \pm 2, \pm 4\}$, depending on the change in anyonic charge. The proposed error is then accepted with probability $\min\{1, e^{-\Delta_{\text{tot}}/k_B T}\}$. If the proposal is accepted, we copy the current state of the system and try to correct it. If correction is successful, we continue our simulation with the uncorrected version of the system. If correction fails (for at least one logical operator), we interpret this as the quantum information having survived for a time which is given by the number of Metropolis steps divided by the number of spins in the system.

The thermal error model has three relevant energy scales $k_B T$, Δ_{\square} , and Δ_{Δ} . Since Δ_{\square} appears in higher-order perturbation theory than Δ_{Δ} , we expect $\Delta_{\Delta} > \Delta_{\square}$. Furthermore, effective protection requires $k_B T < \Delta_{\square}, \Delta_{\Delta}$. We introduce a parameter λ which quantifies the separation of these three energy scales, i.e., $\Delta_{\square} = \lambda k_B T$ and $\Delta_{\Delta} = \lambda^2 k_B T$. Very high values of λ are uninteresting, since they exponentially suppress errors from occurring.

B. Without defects

If there are no defect lines present, the anyonic charge of both types of anyons is conserved (modulo 4), and they can be corrected separately. Various techniques have been developed for correcting general $D(\mathbb{Z}_n)$ quantum double models [27, 41–43]. However, correcting the $D(\mathbb{Z}_4)$ case is particularly easy, since we can exploit the relation $\mathbb{Z}_4/\mathbb{Z}_2 \simeq \mathbb{Z}_2$. Specifically, we can first fuse all oddly-charged anyons in pairs. In a second round, the remaining anyons, which are all of charge 2, are fused in pairs. In order to find these pairings, we use the library **Blossom V** [44], which is the latest implementation of the efficient minimum-weight perfect matching algorithm due to Edmonds [45]. The weight between two equal-type anyons is thereby defined as the minimal number of generalized Pauli operators that need to be applied to create a pair of anyons at the two given locations.

Fig. 6 shows our results for the depolarizing noise model, i.e., the logical error rates of the logical operators \tilde{X}_1 and \tilde{Z}_1 illustrated in Fig. 2 as a function of the depolarization rate p . One clearly recognizes threshold error rates $p_c \approx 24\%$ and $p_c \approx 10\%$, respectively. The equivalent figures for the logical operators \tilde{Z}_2 and \tilde{X}_2 look very similar and yield equivalent threshold error rates p_c .

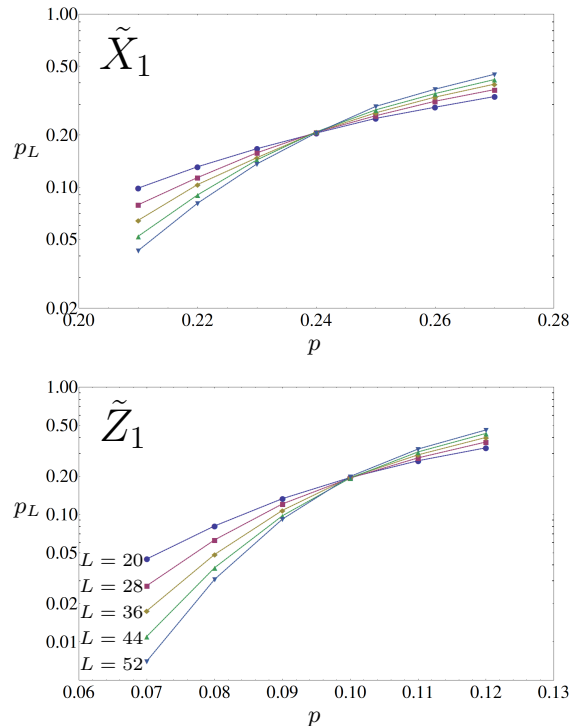


FIG. 6. Error rates p_L of the logical operators \tilde{X}_1 and \tilde{Z}_1 illustrated in Fig. 2 as a function of the qubit depolarization rate p for code sizes $L = 20, 28, 36, 44, 52$. Each data point represents 10^4 logical errors, such that error bars are negligible. We recognize a threshold error rate $p_c \approx 24\%$ for \tilde{X}_1 and $p_c \approx 10\%$ for \tilde{Z}_1 .

These thresholds are best compared with those for an equivalent code based on \mathbb{Z}_2 anyons, and so with only a single qubit on each vertex. For independent bit and phase flips, the thresholds for \tilde{X}_1 and \tilde{Z}_1 are $p_c \approx 16.4\%$ and $p_c \approx 6.7\%$, respectively [46, 47]. When the hexagonal and triangular plaquettes are decoded separately, these correspond to thresholds of $p_c \approx 24.6\%$ and $p_c \approx 10.5\%$ for depolarizing noise. The similarity of these \mathbb{Z}_2 values with those of \mathbb{Z}_4 is remarkable. This qudit code is therefore just as adept at suppressing qubit noise as its qubit counterpart.

It is well-known that the finite-temperature lifetime of a two-dimensional quantum memory with local interactions only is upper-bounded by a constant independent of the system size, see e.g. Ref. [48]. Fig. 7 shows the lifetime of a logical qudit with logical operators X_1 and Z_1 subject to the thermal error model. We notice lifetimes that decrease to an asymptotic value for large L and considerable finite-size tails. These tails correspond to the regime in which the breakdown of error correction is not due to the density of anyons becoming so high that pairing them becomes ambiguous, but where the breakdown is caused by one of the first pairs wandering along a topologically non-trivial path around the torus. The smaller the system, the longer it takes to produce an anyon pair,

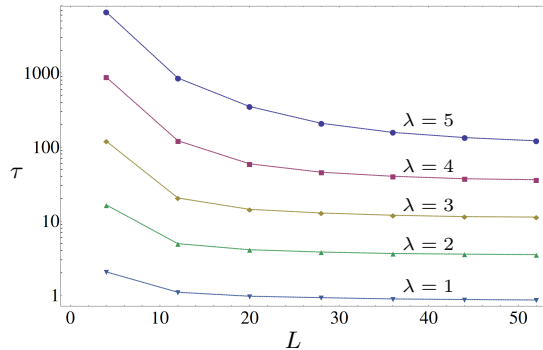


FIG. 7. Average lifetimes τ of the logical qudit with logical operators \tilde{X}_1 and \tilde{Z}_1 as a function of code size L for $\lambda = 1, 2, 3, 4, 5$. Each data point represents 10^4 experiments. The lifetime is defined as the number of Metropolis steps until the first logical operator detects an error, divided by the number of spins in the code.

leading to the observed tails for small enough L and T (large enough λ).

C. With defects

When defect lines as in Fig. 3 are present, the error correction problem becomes more involved. It is no longer possible to correct the two anyon types (hexagons and triangles in our case) separately, as is usually done for the $D(\mathbb{Z}_n)$ models [27, 41–43]. Instead, error correction needs to take the possibility of converting between different anyon types into account. We thus pair all odd-charge anyons of both types in a first round and all remaining charge 2 anyons of both types in a second round. Pairings can involve anyons which are of equal or of different type. The weight for connecting two anyons is defined as the minimal number of generalized Pauli operators needed to create a pair of anyons at their respective positions from the vacuum. For equal-type anyons, this will be an error string that crosses an even number of defect lines, while for different-type anyons this will be an error string that crosses an odd number of defect lines. This can mean, for instance, that connecting two equal-type anyons can have a large weight despite them being geometrically nearby, if there is a defect line between them.

For a code of linear size L in both dimensions, with periodic boundary conditions and L even, we choose defect lines involving $L/2 + 1$ qudits, as shown in Fig. 3 for $L = 20$. The logical operators \tilde{X}_L and \tilde{Z}_L then have a distance $L + 2$ and $L/2 + 4$, respectively.

For the depolarizing error model, we find the threshold error rates p_c for both of the logical operators \tilde{X}_L and \tilde{Z}_L given in Fig. 3. The results are given in Fig. 8. For the defect operator \tilde{X}_L , we find a threshold error rate $p_c \approx 24\%$, as for the operators \tilde{X}_1 and \tilde{X}_2 in the defect-

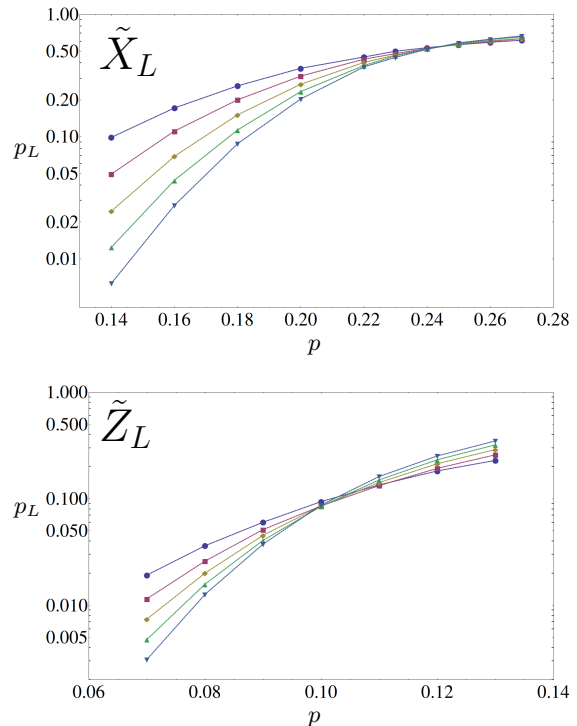


FIG. 8. Error rates p_L of the logical operators \tilde{X}_L and \tilde{Z}_L illustrated in Fig. 3 as a function of the qubit depolarization rate p for code sizes $L = 20, 28, 36, 44, 52$. Each data point represents 10^4 logical errors, such that error bars are negligible. We recognize a threshold error rate $p_c \approx 24\%$ for \tilde{X}_L and $p_c \approx 10\%$ for \tilde{Z}_L .

free case (Figs. 2 and 6), while for the defect operator \tilde{Z}_L we find a threshold error rate $p_c \approx 10\%$, as for the operators \tilde{Z}_1 and \tilde{Z}_2 in the defect-free case.

The fact that these values coincide with the defect free case is not unexpected. The introduction of the defects essentially corresponds to a change in the boundary conditions. However, the vast majority of errors have large support within the bulk. The value of the threshold is therefore dominated by bulk effects rather than boundary effects.

Fig. 9 shows the average lifetime of the qudit stored in the synthetic topological degeneracy in Fig. 3 for the thermal error model. We note that for a given parameter λ , the asymptotic lifetimes ($L \rightarrow \infty$) are close to those in the defect-free case given in Fig. 7.

VII. CONCLUSIONS

We have proposed a system which, on the physical level, involves only nearest-neighbor two-qubit interactions, allows one to perform all Clifford gates through quasi-particle braiding, and has a well-understood error correction problem.

We have greatly benefitted from the fact that our non-

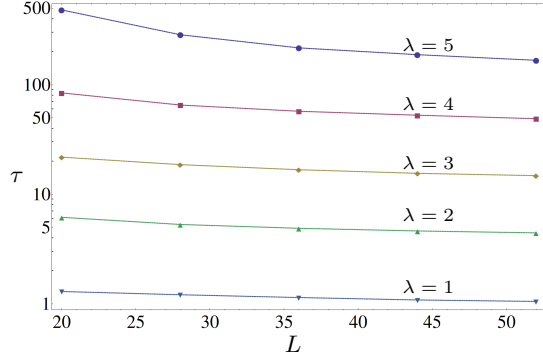


FIG. 9. Average lifetimes τ of the logical qudit stored in the defect logical operators \tilde{X} and \tilde{Z} illustrated in Fig. 3 as a function of code size L for $\lambda = 1, 2, 3, 4, 5$. Each data point represents 10^4 experiments. The lifetime is defined as the number of Metropolis steps divided by the number of spins in the code.

Abelian system is built on top of a system whose excitations correspond to an Abelian anyon model. This allows us to perform the logical operators X , Z , and Λ through quasi-particle braiding. It also makes our error correction problem manageable, despite some subtleties such as the fact that single-spin Pauli operators gener-

ate superpositions between different syndrome outcomes and the ability to convert between different anyon species during error correction.

Universal quantum computation requires the ability to perform non-Clifford gates, such as “small-angle” unitaries. While it is not difficult to perform a non-Clifford operation by non-topological means in our system, this abandons fault-tolerance. The technique of magic state distillation [49] is typically used to restore fault-tolerance. While research on magic state distillation has so far focused on prime qudit dimensions d [50, 51], qudit codes with the right transversality properties to perform magic state distillation in non-prime dimensions, including $d = 4$, also exist [52]. Unfortunately, for non-prime d it is not known whether Clifford gates plus an arbitrary non-Clifford gate are sufficient to achieve universality [53]. It is our hope that our work fuels interest in the $d = 4$ case, being a power of 2 and thus allowing to employ qubits, as demonstrated in our work, while being the smallest power of 2 that allows one to go beyond the Ising/Majorana case.

Alternatively, one could imagine energetically penalizing one of the degrees of freedom of a two-qubit Hilbert space to obtain a synthetic qutrit ($d = 3$). Magic state distillation for qutrits is well-studied [54], potentially allowing to perform fault-tolerant universal quantum computation with \mathbb{Z}_3 parafermions in a qubit system [55].

This work was supported by the SNF, NCCR QSIT, and IARPA.

-
- [1] A. Yu. Kitaev, *Ann. Phys.* **303**, 2–30 (2003).
 - [2] C. Nayak, S. H. Simon, A. Stern, M. Freedman, and S. Das Sarma, *Rev. Mod. Phys.* **80**, 1083 (2008).
 - [3] J. K. Pachos, *Introduction to Topological Quantum Computation*, Cambridge University Press (2012).
 - [4] R. Barends, J. Kelly, A. Megrant, A. Veitia, D. Sank, E. Jeffrey, T. C. White, J. Mutus, A. G. Fowler, B. Campbell, Y. Chen, Z. Chen, B. Chiaro, A. Dunsworth, C. Neill, P. O’Malley, P. Roushan, A. Vainsencher, J. Wenner, A. N. Korotkov, A. N. Cleland, and J. M. Martinis, *Nature* **508**, pp. 500503 (2014).
 - [5] C. Monroe and J. Kim, *Science* **339**, no. 6124, pp. 1164–1169 (2013).
 - [6] Ch. Kloeffel and D. Loss, *Annu. Rev. Condens. Matter Phys.* **4**, 51 (2013).
 - [7] Antonio Negretti, Philipp Treutlein, Tommaso Calarco, *Quantum Inf. Process.* **10**, 721–753 (2011).
 - [8] J. Alicea, *Rep. Prog. Phys.* **75**, 076501 (2012).
 - [9] S. Bravyi, *Phys. Rev. A* **73**, 042313 (2006).
 - [10] M. Freedman, C. Nayak, and K. Walker, *Phys. Rev. B* **73**, 245307 (2006).
 - [11] N. H. Lindner, E. Berg, G. Refael, and A. Stern, *Phys. Rev. X* **2**, 041002 (2012).
 - [12] M. Cheng, *Phys. Rev. B* **86**, 195126 (2012).
 - [13] D. J. Clarke, J. Alicea, and K. Shtengel, *Nat. Commun.* **4**, 1348 (2013).
 - [14] A. Vaezi, *Phys. Rev. B* **87**, 035132 (2013).
 - [15] M. Burrello, B. van Heck, and E. Cobanera, *Phys. Rev. B* **87**, 195422 (2013).
 - [16] R. S. K. Mong, D. J. Clarke, J. Alicea, N. H. Lindner, P. Fendley, C. Nayak, Y. Oreg, A. Stern, E. Berg, K. Shtengel, and M. P.A. Fisher, *Phys. Rev. X* **4**, 011036 (2014).
 - [17] J. Klinovaja and D. Loss, *Phys. Rev. Lett.* **112**, 246403 (2014).
 - [18] F. Zhang and C. L. Kane, *Phys. Rev. Lett.* **113**, 036401 (2014).
 - [19] Y. Oreg, E. Sela, and A. Stern, *Phys. Rev. B* **89**, 115402 (2014).
 - [20] J. Klinovaja and D. Loss, *Phys. Rev. B* **90**, 045118 (2014).
 - [21] J. Klinovaja, A. Yacobi, and D. Loss, *Phys. Rev. B* **90**, 155447 (2014).
 - [22] C. P. Orth, R. P. Tiwari, T. Meng, and T. L. Schmidt, *Phys. Rev. B* **91**, 081406 (2015).
 - [23] H. Bombin, *Phys. Rev. Lett.* **105**, 030403 (2010).
 - [24] Y.-Z. You, C.-M. Jian, and X.-G. Wen, *Phys. Rev. B* **87**, 045106 (2013).
 - [25] J. R. Wootton, J. Burri, S. Iblisdir, and D. Loss, *Phys. Rev. X* **4**, 011051 (2014).
 - [26] C. G. Brell, S. Burton, G. Dauphinais, S. T. Flammia, and D. Poulin, *Phys. Rev. X* **4**, 031058 (2014).
 - [27] A. Hutter, D. Loss, and J. R. Wootton, *New J. Phys.* **17**, 035017 (2015).
 - [28] E. Fradkin and L. P. Kadanoff, *Nucl. Phys. B* **170**, 1 (1980).

- [29] J. Kempe, A. Yu. Kitaev, and O. Regev, SIAM Journal of Computing **35**(5), pp. 1070–1097 (2006).
- [30] S. P. Jordan and E. Farhi, Phys. Rev. A **77**, 06232 (2008).
- [31] R. Oliveira and B. M. Terhal, Quant. Inf. Comp. **8**, No. 10, pp. 900–924 (2008).
- [32] J. K. Pachos and M. B. Plenio, Phys. Rev. Lett. **93**, 056402, (2004).
- [33] H. P. Büchler, A. Micheli, and P. Zoller, Nat. Phys. **3**, pp. 726 – 731 (2007).
- [34] A. Micheli, G. K. Brennen, and P. Zoller, Nat. Phys. **2**, pp. 341 – 347 (2006).
- [35] A. Yu. Kitaev, Ann. Phys. **321**, pp. 2–111 (2006).
- [36] P. Bonderson, M. Freedman, and C. Nayak, Phys. Rev. Lett. **101**, 010501 (2008).
- [37] J. R. Wootton, arXiv:1501.07779 (2015).
- [38] S. Clark, J. Phys. A: Math. Gen. **39**, 2701 (2006).
- [39] J. R. Wootton, V. Lahtinen, B. Boucot, J. K. Pachos, Ann. Phys. **326**, 2307 (2011).
- [40] J. R. Wootton, J. of M. Optics **59**, 20 (2012).
- [41] G. Duclos-Cianci and D. Poulin, Phys. Rev. A **87**, 062338 (2013).
- [42] H. Anwar, B. J. Brown, E. T. Campbell, and D. E. Browne, New J. Phys. **16** 063038 (2014).
- [43] F. H. E. Watson, H. Anwar, and D. E. Browne, arXiv:1411.3028 (2014).
- [44] V. Kolmogorov, Math. Prog. Comp. **1**, 43 (2009).
- [45] J. Edmonds, Can. J. Math. **17**, 449 (1965).
- [46] B. Roethlisberger, J. R. Wootton, R. M. Heath, J. K. Pachos, D. Loss, Phys. Rev. A **85**, 022313 (2012).
- [47] A. Al-Shimary, J. R. Wootton and J. K. Pachos, New J. Phys. **15** 025027 (2013).
- [48] B. J. Brown, D. Loss, J. K. Pachos, C. N. Self, J. R. Wootton, arXiv:1411.6643 (2014).
- [49] S. Bravyi and A. Kitaev, Phys. Rev. A **71**, 022316 (2005).
- [50] E. T. Campbell, H. Anwar, and D. E. Browne, Phys. Rev. X **2**, 041021 (2012).
- [51] E. T. Campbell, Phys. Rev. Lett. **113**, 230501 (2014).
- [52] F. H. E. Watson, E. T. Campbell, H. Anwar, and D. E. Browne, arXiv:1503.08800 (2015).
- [53] E. T. Campbell, private communication.
- [54] H. Anwar, E. T. Campbell, and D. E. Browne, New J. Phys. **14** 063006 (2012).
- [55] This is indeed a route we have tentatively followed. Unfortunately, the Hamiltonians necessary to generate $D(\mathbb{Z}_3)$ quantum double models in a qubit system turned out to be much more involved than Eq. (4).
- [56] J. R. Schrieffer and P. A. Wolff, Phys. Rev. **149**, 491 (1966).
- [57] S. Bravyi, D. P. DiVincenzo, and D. Loss, Ann. Phys. **326**, No. 10, pp. 2793–2826 (2011).
- [58] Note that, for closed boundary conditions, this added degeneracy does not arise for the first pair to be unpaired.

Appendix A: Sixth-order degenerate perturbation theory

For our perturbation theory, we employ a Schrieffer-Wolff transformation [56], as formalized in Ref. [57].

Consider an unperturbed Hamiltonian H_0 whose spectrum can be separated into a low- and a high-energy subspace, which are energetically separated by a gap. Given a perturbation V , we want to find an effective Hamiltonian H_{eff} describing the “effective” physics on the low-energy subspace. The effective Hamiltonian can be developed in a perturbative series

$$H_{\text{eff}} = H_{\text{eff}}^{(0)} + H_{\text{eff}}^{(1)} + H_{\text{eff}}^{(2)} + \dots \quad (\text{A1})$$

in powers of some small expansion parameter.

Let P denote the projector onto the low-energy subspace and $Q = \mathbb{1} - P$ the projector onto the high-energy subspace. We define $V_d = PVP + QVQ$ and $V_{\text{od}} = V - V_d = PVQ + QVP$. For some operator A , we define the superoperator \hat{A} via $\hat{A}(O) = [A, O]$. Let $H_0 = \sum_i E_i |i\rangle\langle i|$ be the spectral decomposition of H_0 and define the superoperator \mathcal{L} via

$$\mathcal{L}(O) = \sum_{i,j} \frac{\langle i|QOP|j\rangle}{E_i - E_j} |i\rangle\langle j| - \text{H.c.} \quad (\text{A2})$$

We employ the convention that unless indicated otherwise by use of brackets, a superoperator \mathcal{L} acts on all operators to its right.

For the sixth-order effective Hamiltonian, one derives from Ref. [57] the expression

$$H_{\text{eff}}^{(6)} = \frac{1}{2} P \hat{S}_5 (V_{\text{od}}) P - \frac{1}{24} P (\hat{S}_1^2 \hat{S}_3 + \hat{S}_1 \hat{S}_3 \hat{S}_1 + \hat{S}_3 \hat{S}_1^2 + \hat{S}_2^2 \hat{S}_1 + \hat{S}_2 \hat{S}_1 \hat{S}_2 + \hat{S}_1 \hat{S}_2^2) (V_{\text{od}}) P + \frac{1}{240} P \hat{S}_1^5 (V_{\text{od}}) P, \quad (\text{A3})$$

where

$$\begin{aligned} S_1 &= \mathcal{L}(V_{\text{od}}) \\ S_2 &= -\mathcal{L}\hat{V}_d(S_1) \\ S_3 &= -\mathcal{L}\hat{V}_d(S_2) + \frac{1}{3} \mathcal{L}\hat{S}_1^3(V_{\text{od}}) \\ S_4 &= -\mathcal{L}\hat{V}_d(S_3) + \frac{1}{3} \mathcal{L}(\hat{S}_1 \hat{S}_2 + \hat{S}_2 \hat{S}_1)(V_{\text{od}}) \\ S_5 &= -\mathcal{L}\hat{V}_d(S_4) + \frac{1}{3} (\hat{S}_2^2 + \hat{S}_1 \hat{S}_3 + \hat{S}_3 \hat{S}_1)(V_{\text{od}}) \\ &\quad - \frac{1}{45} \mathcal{L}\hat{S}_1^4(V_{\text{od}}). \end{aligned} \quad (\text{A4})$$

In our case, the low-energy subspace onto which P projects is given by the space in which all triangle operators in Eq. (8) have minimal energy, i.e., $Z_a Z_b Z_c \equiv 1$ for all triangles (a, b, c) . This subspace is fully degenerate. The lowest-energetic excitations change the eigenvalue of a stabilizer $Z_a Z_b Z_c$ from 1 to $\pm i$. Since the eigenvalue of $-(Z_a Z_b Z_c + \text{H.c.})$ is thereby changed from -2 to 0 , this has an energy cost $\Delta = 2J$. Note, however, that stabilizer eigenvalues can only be changed in pairs, such that the gap between the low-energetic (ground-state) subspace and the space of excited states is in fact given by 2Δ .

A crucial property of our Hamiltonian is that there is no lower-than-sixth-order perturbation that acts within the groundstate space. Therefore, we are only interested in terms of the form $PV_{\text{od}}(V_d)^4 V_{\text{od}}P$, which allows to greatly simplify the effective Hamiltonian. Namely, only the first summand in all expressions in Eqs. (A3) and (A4) is relevant in our case. We find

$$H_{\text{eff}}^{(6)} = \frac{1}{2} P \left[(\mathcal{L}\hat{V}_d)^4 (\mathcal{L}V_{\text{od}}), V_{\text{od}} \right] P. \quad (\text{A5})$$

$0 \rightarrow 2\Delta \rightarrow 2\Delta \rightarrow 2\Delta \rightarrow 2\Delta \rightarrow 2\Delta \rightarrow 0$	96
$0 \rightarrow 2\Delta \rightarrow 4\Delta \rightarrow 2\Delta \rightarrow 2\Delta \rightarrow 2\Delta \rightarrow 0$	48
$0 \rightarrow 2\Delta \rightarrow 2\Delta \rightarrow 4\Delta \rightarrow 2\Delta \rightarrow 2\Delta \rightarrow 0$	48
$0 \rightarrow 2\Delta \rightarrow 2\Delta \rightarrow 2\Delta \rightarrow 4\Delta \rightarrow 2\Delta \rightarrow 0$	48
$0 \rightarrow 2\Delta \rightarrow 4\Delta \rightarrow 4\Delta \rightarrow 2\Delta \rightarrow 2\Delta \rightarrow 0$	96
$0 \rightarrow 2\Delta \rightarrow 2\Delta \rightarrow 4\Delta \rightarrow 4\Delta \rightarrow 2\Delta \rightarrow 0$	96
$0 \rightarrow 2\Delta \rightarrow 4\Delta \rightarrow 4\Delta \rightarrow 4\Delta \rightarrow 2\Delta \rightarrow 0$	192
$0 \rightarrow 2\Delta \rightarrow 4\Delta \rightarrow 2\Delta \rightarrow 4\Delta \rightarrow 2\Delta \rightarrow 0$	24
$0 \rightarrow 2\Delta \rightarrow 4\Delta \rightarrow 6\Delta \rightarrow 4\Delta \rightarrow 2\Delta \rightarrow 0$	72

TABLE II. Possible routes the excitation energy above the groundstate can take (left column), together with their respective multiplicities (right column). Note that the number of multiplicities adds up to $6! = 720$.

Using now that in our case $V_d P = 0$, this can be further simplified to

$$\begin{aligned} H_{\text{eff}}^{(6)} &= \frac{1}{2} P \mathcal{L} (\mathcal{L} (\mathcal{L} (\mathcal{L} (\mathcal{L} (V_{\text{od}}) V_d) V_d) V_d) V_d) V_{\text{od}} P \\ &\quad - \frac{1}{2} P V_{\text{od}} (\mathcal{L} V_d)^4 (\mathcal{L} V_{\text{od}}) P \\ &= -P V_{\text{od}} (\mathcal{L} V_d)^4 (\mathcal{L} V_{\text{od}}) P. \end{aligned} \quad (\text{A6})$$

There are $6! = 720$ possibilities for applying the six factors $X_r X_s^\dagger X_t X_u^\dagger X_v X_w^\dagger$ around one hexagon which leads the system back to the groundstate. Table II lists all possible routes the excitation energy above the groundstate can take, together with their numbers of possibilities.

In conclusion, we find the sixth-order effective Hamiltonian

$$H_{\text{eff}} = -q \frac{h^6}{\Delta^5} (X_r X_s^\dagger X_t X_u^\dagger X_v X_w^\dagger + \text{H.c.}), \quad (\text{A7})$$

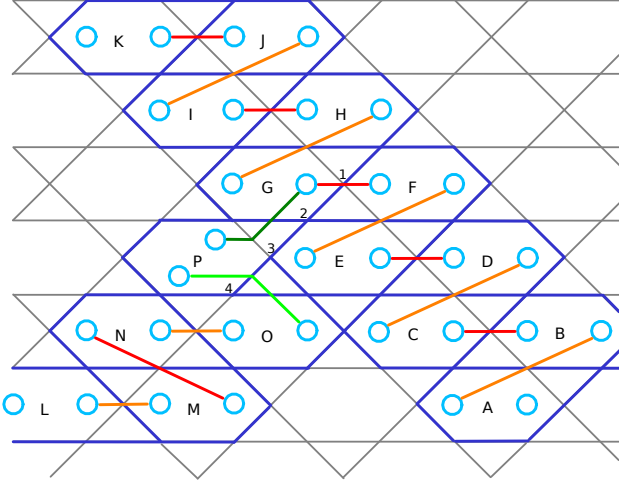


FIG. 10. A selection of double plaquettes used in a braiding operation.

where the dimensionless prefactor

$$\begin{aligned}
 q &= \frac{96}{32} + \frac{48}{64} + \frac{48}{64} + \frac{48}{64} + \frac{96}{128} + \frac{96}{128} \\
 &\quad + \frac{192}{256} + \frac{24}{128} + \frac{72}{384} \\
 &= \frac{63}{8}
 \end{aligned} \tag{A8}$$

is given by the multiplicities in Table II, divided by the product of all excitation energies (in multiples of Δ) along the virtual process.

Appendix B: Moving unpaired parafermion modes

To consider the creation and braiding of unpaired parafermionic modes, we must first decide on the double plaquettes with which we will work. Let us consider those of Fig. 10. To visualize the two parafermion modes within each double plaquette we use light blue circles. The one to the right of a double plaquette P is labelled P_1 , and that to the left is P_2 .

Parity operators for ψ modes are defined on pairs of parafermion modes. We are primarily concerned with two types of pairing: those of the two modes within the same double plaquette, and those of two modes from neighbouring double plaquettes. Relevant examples of the latter type are shown in Fig. 10 by red, orange and green lines connecting the corresponding modes.

For the two modes within each double plaquette, the parity operator $\omega^{3/2}\gamma_{P_1}\gamma_{P_2}^\dagger$ corresponds to the stabilizer S_P . The orange and red lines connecting modes P_2 to $(P+1)_1$ denote the parity operators $\omega^{3/2}\gamma_{P_2}\gamma_{(P+1)_1}^\dagger$. For orange lines, these correspond to the operator Y on the vertex through which the line passes. For red lines they correspond to the operator $X^\dagger Z$.

Consider a state initially within the stabilizer space. The parity operators for the pairs of parafermion modes within each double plaquette are therefore part of the stabilizer. The state therefore corresponds to this definite pairing of the modes.

Let us now consider the removal of the operator S_A from the set of stabilizer generators (while W_A remains). The corresponding parafermion modes are now, in some sense, unpaired. This contributes a factor of four to the ground space degeneracy [58]. However, due to the fact that the ‘unpaired’ parafermions are not well separated, it is not difficult for local perturbations to lift the degeneracy of this space. To become truly unpaired, and benefit from topological protection, they must be separated.

To do this, we can add a term $K(Y + Y^\dagger)$ to the Hamiltonian, which corresponds to the parity operator $\omega^{3/2}\gamma_{A_2}\gamma_{B_1}^\dagger$. This acts on the vertex through which the orange line connecting these modes passes.

For $K \gg J$, this new term will overwhelm the S_B term. The pairing of B_1 and B_2 will then be broken, and B_1 will become paired with A_2 instead. The unpaired mode originally at A_2 is therefore effectively moved to B_2 . If the new term is introduced adiabatically, the degenerate subspace associated with the unpaired parafermion modes will remain in the same state during this process.

Similar processes can be used to move the unpaired modes further. The Hamiltonian term $K(X^\dagger Z + X^\dagger Z)$ corresponding to $\omega^{3/2}\gamma_{B_2}\gamma_{A_1}^\dagger$ can then be used to move the parafermion at B_2 to C_2 , for example. Unpaired parafermion modes can therefore be separated by arbitrary distances, at the endpoints of lines on which single qudit terms are added to the Hamiltonian. In terms of qubits, these correspond to two-body interactions between qubits in the same site.

In order to unlock the potential of parafermions for quantum computation, it must be possible to braid the parafermion modes. Let us consider a specific example of this, using the system of Fig. 10. Consider an initial state within the stabilizer space of all S_P except A and L . At these two points, we have the unpaired parafermion modes A_1, A_2, L_1 and L_2 . Let us now consider operations such as those described above to move A_1 and L_2 away, beyond the bottom of the figure. All four parafermion modes are then well separated, and so the ground state degeneracy is topological protected.

We will now consider the exchange of A_2 with L_1 . We do this by first moving A_2 to K_2 , then L_1 to A_2 , and finally K_2 to L_1 . The two modes have then swapped places. An exchange of opposite chirality would correspond to first moving L_1 to K_1 , and so on. Note that all modes are kept well separated during the exchange, and so topological protection is always maintained.

During the exchange, the movement of the modes is mostly achieved using Hamiltonian terms that correspond to the red and orange pairings in Fig. 10. These are all single qudit terms. At the junction, however, terms corresponding to the green pairings are used. We must

therefore consider these in detail.

For the pairing shown by the light green line, the parity operator is $\omega^{3/2}\gamma_{P_2}\gamma_{O_1}^\dagger$. This has the effect of creating an ψ_g, ψ_{-g} pair on the double plaquettes O and P . This requires the two qudit operator $X_3^\dagger X_4 Z_4^\dagger$. For the dark green pairing, the $\omega^{3/2}\gamma_{P_1}\gamma_{G_2}^\dagger$ parity operator similarly requires the three qudit operator $X_1 X_2^\dagger Z_2 Z_3$. These terms correspond to four- and six-body quasi-local interactions on the corresponding qubits, respectively. They can be realized by standard methods of perturbative gadgets. However, note that they need only be implemented while an exchange is in progress.

Appendix C: Exchange of two parafermion modes

To determine the effects of a single exchange we consider the smallest possible implementation. This involves the double plaquettes labelled F, G and P in Fig. 10. We consider a state in which the modes at P_1 and F_2 are unpaired, and those at G_1 and G_2 are paired by the Hamiltonian term S_G . Using this, we determine the effects of exchanging the unpaired modes.

The results of the exchange are most easily understood in terms of the ψ mode formed by this pair. The parity operator, Γ for this mode is an operator that creates a ψ_1, ψ_{-1} pair and places them in double plaquettes P and F , respectively. Also it must have eigenvalues of the form ω^g , and so $\Gamma^4 = 1$. These conditions are satisfied by

$$\Gamma = \omega^{(1+2a)/2} Z_1 X_2^\dagger Z_2 Z_3. \quad (C1)$$

We similarly require operations that can move parafermions between the relevant plaquettes. These correspond to the green line between G and P and the red line between F and G . These are

$$\Pi = \omega^{(1+2b)/2} X_1 X_2^\dagger Z_2 Z_3, \quad \Phi = \omega^{(1+2c)/2} X_1^\dagger Z_1, \quad (C2)$$

respectively. In these relations a, b and c are all elements of \mathbb{Z}_4 .

We have freedom in choosing the values $a, b, c \in \mathbb{Z}_4$ for these relations. The corresponding freedom also exists for all operators used to move parafermion modes, as well as the logical operators. The values used do not simply correspond to differences in a global phase. Instead they determine which eigenspace of these operators has eigenvalue $\omega^0 = 1$, and so which one corresponds to the vacuum occupancy ψ_0 of the ψ mode. These phases therefore cannot be chosen entirely arbitrarily, since the overall conservation constraint of ψ modes must be maintained. However, since here we do not explicitly consider the operations that placed unpaired parafermion modes at P_1 and F_2 , we can assume that their phases are chosen in a way that maintains this conservation. We will therefore consider a free choice of a, b , and c .

The first step in exchanging the parafermions is to move the one at P_1 to G_2 . This is done by adiabatically changing the Hamiltonian to one in which the term

$\Pi + \Pi^\dagger$ is present and stronger than S_G . This causes the modes at G_1 and P_1 to pair, moving the mode once at P_1 to G_2 . The mode at F_2 is then moved to that at P_1 by adiabatically changing the Hamiltonian to one in which the $\Phi + \Phi^\dagger$ term is present and stronger than S_G , and the $\Pi + \Pi^\dagger$ term is removed, pairing F_2 with G_1 . The mode at G_2 is then moved to P_1 by adiabatically removing the $\Pi + \Pi^\dagger$ term and so allowing S_G to become dominant and G_1 and G_2 to pair. This process then results in the clockwise exchange of the modes.

The first step of this transformation takes a state that is initially in the ω^0 eigenspace of S_G and projects it to one in the ω^0 eigenspace of Φ . The next step projects the state into the ω^0 eigenspace of Π . The final step projects back into the ω^0 eigenspace of S_G . The end effect is then $P_G P_\Phi P_\Pi P_G$. Here P_G is the projector onto the ω^0 eigenspace of S_G , etc. The rightmost P_G simply reflects the fact that the initial state lies within this eigenspace.

The parity operator Γ for the pair of unpaired modes commutes with S_G , and so can be mutually diagonalized with the above operator. We can therefore interpret its effects in terms of the phase factor assigned to each of the possible ψ_g eigenspaces of the ψ mode of the pair. For $a = 0$ and $b = c = 1$, the phase assigned to ψ_g is $\omega^{g^2/2}$, up to a global phase of $\sqrt{-\omega}$.

For other values of a, b , and c , the results obtained will be different. This may seem to contradict the standard notion of a topological protected operation. However, these differences can be most easily understood by considering movement of parafermion modes implemented by measurement rather than adiabatic Hamiltonian manipulation. This method forces pairing of parafermion modes by measuring the occupancy of their corresponding ψ mode, and so forcing it to have a definite value. Ideally, this measurement will give the vacuum result ψ_0 . The effect is then the same as the adiabatic manipulation. If a different ψ_g results, it must be removed by fusing it with the unpaired parafermion mode being moved. The different values used for the phases when moving unpaired modes, such as a, b and c here, determine how the measurement results are interpreted in terms of ψ anyons, and so determine the net ψ_g fused with the modes being moved. As such, differences in the conventions used for an exchange will change the resulting operation only by a factor of Γ^g , for some value of g that depends on a, b , and c .

Appendix D: Generators of the Clifford group

For a tensor product of n d -level systems $(\mathbb{C}^d)^{\otimes n}$, the Pauli group \mathcal{P}_d is defined as the group generated by the generalized Pauli operators X_i and Z_i , and the Clifford group \mathcal{C}_d is defined as the centralizer of \mathcal{P}_d in the unitary group on $(\mathbb{C}^d)^{\otimes n}$. That is, elements in \mathcal{C}_d map tensor products of d -level Pauli operators to other such tensor products under conjugation.

We start with some general remarks on the action

of $\mathcal{C}_d^{\otimes n}$ on $\mathcal{P}_d^{\otimes n}$ for $d = 4$. For $d = 4$, an operator $X^a Z^b$ has eigenvalues $\{1\}$ if $a = b = 0$, $\{1, -1\}$ if both a and b are even and at least one of them is non-zero, $\{i^{1/2}, i^{3/2}, i^{5/2}, i^{7/2}\}$ if both a and b are odd, and $\{1, i, -1, -i\}$ if $a + b$ is odd. Since the number of distinct eigenvalues is preserved under conjugation, this implies that the Pauli group $\mathcal{P}_d^{\otimes n}$ decays into distinct orbits when $\mathcal{C}_d^{\otimes n}$ acts on it by conjugation. This is in stark contrast to the case where d is an odd prime, which is studied in Ref. [38], where there is only one non-trivial orbit. The orbit containing the elements $X_1, Z_1, \dots, X_n, Z_n$ consists of elements of the form

$$\omega^{k+p/2} Z_1^{a_1} X_1^{b_1} \dots Z_n^{a_n} X_n^{b_n}, \quad (\text{D1})$$

where $k, a_1, b_1, \dots, a_n, b_n \in \mathbb{Z}_4$, at least one of the exponents $a_1, b_1, \dots, a_n, b_n$ is odd, and $p = \sum_{i=1}^n a_i b_i$ determines whether integer or half-integer powers of ω appear as phases (we sometimes write ω for i to avoid confusion with indices).

The following proof is an adaption of the proof in Appendix A of Ref. [38], where it is shown that a certain set of gates generate the Clifford group $\mathcal{C}_d^{\otimes n}$ for the case where d is an odd prime. The general structure of our proof is identical to the one in Ref. [38], while the generating set and individual lemmas and their proofs are different.

Let us define the single-qudit unitaries

$$H = \frac{1}{2} \sum_{j,k=1}^4 \omega^{jk} |j\rangle \langle k| \quad (\text{D2})$$

$$S = \sum_{j=1}^4 \omega^{j^2/2} |j\rangle \langle j|, \quad (\text{D3})$$

and

$$T = \frac{1}{2} \begin{pmatrix} \sqrt{i} & 1 & -\sqrt{i} & 1 \\ 1 & \sqrt{i} & 1 & -\sqrt{i} \\ -\sqrt{i} & 1 & \sqrt{i} & 1 \\ 1 & -\sqrt{i} & 1 & \sqrt{i} \end{pmatrix}. \quad (\text{D4})$$

Lemma 1. *The gates $S^\dagger, T^\dagger, Z^\dagger, X, X^\dagger$, and $\sqrt{i}H$ can all be generated from S, T , and Z .*

Proof. As $S^8 = T^8 = \mathbb{1}$, we have $S^\dagger = S^7$ and $T^\dagger = T^7$. We have $\sqrt{i}H = STS = TST$ and $X = H^\dagger ZH = (\sqrt{i}H)^\dagger Z(\sqrt{i}H)$. Finally, $X^4 = Z^4 = \mathbb{1}$, so $X^\dagger = X^3$ and $Z^\dagger = Z^3$. \square

If for some Clifford gate $U \in \mathcal{C}_d^{\otimes n}$ we have

$$U(Z_1^{a_1} X_1^{b_1} \dots Z_n^{a_n} X_n^{b_n})U^\dagger = \alpha Z_1^{a'_1} X_1^{b'_1} \dots Z_n^{a'_n} X_n^{b'_n}, \quad (\text{D5})$$

with $|\alpha| = 1$, we write

$$M(U)(a_1, b_1, \dots, a_n, b_n)^T = (a'_1, b'_1, \dots, a'_n, b'_n)^T. \quad (\text{D6})$$

The matrices $M(U) \in \mathbb{Z}_d^{2n \times 2n}$ form a representation of $\mathcal{C}_d^{\otimes n}$, as $M(UV) = M(U)M(V)$.

Lemma 2. *The gates S, T , and Z generate the entire single-qudit Clifford group $\mathcal{C}_4^{\otimes 1}$.*

Proof. For some $U \in \mathcal{C}_4^{\otimes 1}$, let $M(U) = \begin{pmatrix} a & c \\ b & d \end{pmatrix}$. Preserving the commutation relations of the single-qudit Pauli operators requires that $ad - bc = 1 \pmod{4}$. One verifies that there are only 48 matrices M in the matrix ring $\mathbb{Z}_4^{2 \times 2}$ satisfying the requirement $\det M = 1 \pmod{4}$. We have $SXS^\dagger = \sqrt{\omega}XZ$ and $TZT^\dagger = \sqrt{\omega}ZX^\dagger$, such that $M(S) = \begin{pmatrix} 0 & 1 \\ 1 & 1 \end{pmatrix}$ and $M(T) = \begin{pmatrix} -1 & 1 \\ 1 & 0 \end{pmatrix}$. One can verify by brute force that products of at most 9 factors $M(S)$ and $M(T)$ generate all of the aforementioned 48 matrices. Finally, since $XZX^\dagger = \bar{\omega}Z$ and $ZXZ^\dagger = \omega X$, we can generate arbitrary phases compatible with Eq. (D1) (for $n = 1$). \square

We define the controlled Pauli-operators

$$C_X = \sum_{j=0}^3 |j\rangle \langle j| \otimes X^j \quad (\text{D7})$$

and

$$C_Z = \sum_{j=0}^3 |j\rangle \langle j| \otimes Z^j = \sum_{j,k=0}^3 \omega^{jk} |j\rangle \langle j| \otimes |k\rangle \langle k|. \quad (\text{D8})$$

Note that C_Z has been called Λ in the main part of this work. We write $A \mapsto_U B$ as a shorthand for $UAU^\dagger = B$.

We have

$$\begin{aligned} Z_1 &\mapsto_{C_X} Z_1 \\ X_1 &\mapsto_{C_X} X_1 X_2 \\ Z_2 &\mapsto_{C_X} Z_1^\dagger Z_2 \\ X_2 &\mapsto_{C_X} X_2 \end{aligned} \quad (\text{D9})$$

and

$$\begin{aligned} Z_1 &\mapsto_{C_Z} Z_1 \\ X_1 &\mapsto_{C_Z} X_1 Z_2 \\ Z_2 &\mapsto_{C_Z} Z_2 \\ X_2 &\mapsto_{C_Z} Z_1 X_2, \end{aligned} \quad (\text{D10})$$

showing that $C_X, C_Z \in \mathcal{C}_4^{\otimes 2}$.

Lemma 3. *The gate C_X can be generated from S, T , and C_Z .*

Proof. We note that

$$H X H^\dagger = Z \quad \text{and} \quad H Z H^\dagger = X^\dagger. \quad (\text{D11})$$

Thus

$$C_X = H_2^\dagger C_Z H_2 = (\sqrt{i}H_2)^\dagger C_Z (\sqrt{i}H_2), \quad (\text{D12})$$

which together with Lemma 1 completes the proof. \square

Let us define a more general controlled operator as

$$C_{st} = S_1^{-st} (C_X)^s (C_Z)^t. \quad (D13)$$

It acts by conjugation as

$$\begin{aligned} Z_1 &\mapsto_{C_{st}} Z_1 \\ X_1 &\mapsto_{C_{st}} \omega^{st/2} X_1 X_2^s Z_2^t \\ Z_2 &\mapsto_{C_{st}} Z_1^{-s} Z_2 \\ X_2 &\mapsto_{C_{st}} Z_1^t X_2. \end{aligned} \quad (D14)$$

Up to the phase $\omega^{st/2}$, this action is identical to the one of the conditional Pauli gate $C_{X^s Z^t}$ studied in Ref. [38]. We point out again that such a phase is unavoidable for \mathbb{Z}_4 , as there is, for instance, no unitary U such that $X_1 \mapsto_U X_1 X_2 Z_2$, since these two operators are not isospectral.

Let us define the SWAP gate \mathcal{S} via $\mathcal{S}|j\rangle|k\rangle = |k\rangle|j\rangle$. Evidently, it acts as

$$X_1 \mapsto_{\mathcal{S}} X_2, \quad Z_1 \mapsto_{\mathcal{S}} Z_2, \quad X_2 \mapsto_{\mathcal{S}} X_1, \quad Z_2 \mapsto_{\mathcal{S}} Z_1. \quad (D15)$$

The gate \mathcal{S} thus allows to generate non-local entangling gates from nearest-neighbor ones.

Lemma 4. *The gate $i\mathcal{S}$ can be generated from S , T , and C_Z .*

Note that the gates \mathcal{S} and $i\mathcal{S}$ act identically by conjugation.

Proof. Let

$$C_{X(1,2)} = \sum_{j=0}^3 |j\rangle\langle j| \otimes X^j, \quad C_{X(2,1)} = \sum_{j=0}^3 X^j \otimes |j\rangle\langle j|. \quad (D16)$$

One verifies that

$$C_{X(1,2)} C_{X(2,1)}^\dagger C_{X(1,2)} (\sqrt{i} H_2)^2 = i\mathcal{S}, \quad (D17)$$

which together with Lemmas 1 and 3 completes the proof. \square

Let

$$\begin{aligned} P &= \alpha_P Z_1^{a_1} X_1^{b_1} \dots Z_n^{a_n} X_n^{b_n} \\ Q &= \alpha_Q Z_1^{c_1} X_1^{d_1} \dots Z_n^{c_n} X_n^{d_n}. \end{aligned} \quad (D18)$$

All arithmetics involving the exponents a_j , b_j , c_j , and d_j that follow are to be understood modulo 4. It follows from the commutation relation $ZX = \omega XZ$ that $PQ = \omega^{(P,Q)} QP$ where

$$(P, Q) = \sum_{i=1}^n a_i d_i - b_i c_i. \quad (D19)$$

Lemma 5. *Given $P, Q \in \mathcal{P}_4^{\otimes n}$ with $(P, Q) = 1$, we can generate $U \in \mathcal{C}_4^{\otimes n}$ from S , T , and nearest-neighbor C_Z such that*

$$\begin{aligned} P &\mapsto_U \alpha_P Z^{a'_1} X^{b'_1} \dots Z^{a'_n} X^{b'_n} \\ Q &\mapsto_U \alpha_Q Z^{c'_1} X^{d'_1} \dots Z^{c'_n} X^{d'_n}, \end{aligned} \quad (D20)$$

with $|\alpha_P| = |\alpha_Q| = 1$, and there exists $j \in \{1, \dots, n\}$ such that $a'_j d'_j - b'_j c'_j = 1$.

Proof. Let P and Q be as in Eq. (D18). Since

$$\sum_{i=1}^n a_i d_i - b_i c_i = 1 \quad (D21)$$

by assumption, there exists j such that

$$r_j = a_j d_j - b_j c_j \in \{+1, -1\}. \quad (D22)$$

If $r_j = 1$, we are done. If $r_j = -1$, then there is $k \neq j$ with $r_k = 2$ or $r_k = -1$. From Lemma 2, we know that from S_i and T_i we can generate single-qudit unitaries that change $\begin{pmatrix} a_i & c_i \\ b_i & d_i \end{pmatrix}$ in arbitrary ways as long as $r_i = a_i d_i - b_i c_i$ is preserved. So up to gates that can be generated from S_j and T_j , we can assume that $a_j = 0$, $b_j = c_j = 1$, and $d_j = 0$. If $r_k = 2$ then, up to gates that can be generated from S_k and T_k , we can assume that $a_k = 1$, $b_k = c_k = 0$, and $d_k = 2$. Finally, if $r_k = -1$ then, up to gates that can be generated from S_k and T_k , we can assume that $a_k = 1$, $b_k = 1$, $c_k = -1$, and $d_k = 2$. We note that application of a phase-gate $C_{Z(j,k)}$ changes r_j to $r'_j = r_j + (b_k d_j - b_j d_k)$, and recall that non-local phase gates $C_{Z(j,k)}$ can be generated from nearest-neighbor ones and SWAP gates, which we can generate according to Lemma 4. In both cases ($r_k = 2$ and $r_k = -1$), we find that application of a phase-gate $C_{Z(j,k)}$ gives $r'_j = 1$. \square

Lemma 6. *Given $P, Q \in \mathcal{P}_4^{\otimes n}$ with $(P, Q) = 1$, we can generate $U \in \mathcal{C}_4^{\otimes n}$ from S , T , and nearest-neighbor C_Z such that*

$$P \mapsto_U Z \otimes P' \quad \text{and} \quad Q \mapsto_U X \otimes Q', \quad (D23)$$

with $P', Q' \in \mathcal{P}_4^{\otimes n-1}$.

Proof. Let P and Q be as in Eq. (D18). By Lemma 5, we can assume that there is j with $a_j d_j - b_j c_j = 1$. Employing Lemma 4, we can perform a SWAP between qudits 1 and j . Finally, we perform a single-qudit unitary L on qudit 1 which is such that $M(L) = \begin{pmatrix} d_j & -c_j \\ -b_j & a_j \end{pmatrix}$. As $\det M(L) = 1 \pmod{4}$, such a unitary L can be constructed from S and T according to Lemma 2. We note that

$$Z^{a_j} X^{b_j} \mapsto_L \alpha_Z Z \quad \text{and} \quad Z^{c_j} X^{d_j} \mapsto_L \alpha_X X, \quad (D24)$$

with $|\alpha_X| = |\alpha_Z| = 1$, which completes the proof. \square

Lemma 7. For any $V \in \mathcal{C}_4^{\otimes n}$ we can construct U from S , T , and nearest-neighbor C_Z such that $UX_1U^\dagger = VX_1V^\dagger$ and $UZ_1U^\dagger = VZ_1V^\dagger$.

Proof. Clearly,

$$(VZ_1V^\dagger, VX_1V^\dagger) = (Z_1, X_1) = 1, \quad (\text{D25})$$

so by Lemma 6, we can assume that $VX_1V^\dagger = X \otimes P'$ and $VZ_1V^\dagger = Z \otimes Q'$, up to gates that can be constructed from S , T , and nearest-neighbor C_Z .

Now let

$$\begin{aligned} P' &= \alpha_P Z_2^{a_2} X_2^{b_2} \dots Z_n^{a_n} X_n^{b_n} \\ Q' &= \alpha_Q Z_2^{c_2} X_2^{d_2} \dots Z_n^{c_n} X_n^{d_n}. \end{aligned} \quad (\text{D26})$$

We define

$$C_{st,i} = S_1^{-st} (C_{X(1,i)})^s (C_{Z(1,i)})^t, \quad (\text{D27})$$

with $i \in \{2, \dots, n\}$. The gate

$$U = (\sqrt{i}H_1)U_Q(\sqrt{i}H_1)^\dagger U_P, \quad (\text{D28})$$

with

$$U_P = \prod_{i=2}^n C_{b_n a_n, i} \quad \text{and} \quad U_Q = \prod_{i=2}^n C_{d_n c_n, i}, \quad (\text{D29})$$

can be constructed from S , T , and nearest-neighbor C_Z according to Lemmas 1, 3 and 4.

Using Eqs. (D11) and (D14), we find the sequences of mappings

$$\begin{aligned} X_1 &\mapsto_{U_P} X \otimes P' \mapsto_{(\sqrt{i}H_1)^\dagger} Z^\dagger \otimes P' \\ &\mapsto_{U_Q} Z^{-1 - \sum_{i=2}^n (a_i d_i - b_i c_i)} \otimes P' \\ &\mapsto_{\sqrt{i}H_1} X^{1 + \sum_{i=2}^n (a_i d_i - b_i c_i)} \otimes P', \end{aligned} \quad (\text{D30})$$

and

$$Z_1 \mapsto_{U_P} Z_1 \mapsto_{(\sqrt{i}H_1)^\dagger} X_1 \mapsto_{U_Q} X \otimes Q' \mapsto_{\sqrt{i}H_1} Z \otimes Q' \quad (\text{D31})$$

where α_P and α_Q in Eq. (D26) are products of all the phases that occur according to Eq. (D14). Since

$$\begin{aligned} 1 &= (Z_1, X_1) = (VZ_1V^\dagger, VX_1V^\dagger) = (Z \otimes Q', X \otimes P') \\ &= 1 + \sum_{i=2}^n (a_i d_i - b_i c_i), \end{aligned} \quad (\text{D32})$$

we finally conclude that

$$\begin{aligned} X_1 &\mapsto_U X \otimes P' = VX_1V^\dagger \\ Z_1 &\mapsto_U Z \otimes Q' = VZ_1V^\dagger, \end{aligned} \quad (\text{D33})$$

as required. \square

Theorem 1. Any Clifford gate $V \in \mathcal{C}_4^{\otimes n}$ can be constructed from S , T , Z , and nearest-neighbor C_Z .

Proof. The proof is done by induction over n . The case $n = 1$ is given by Lemma 2. For $n > 1$, let U be as in Lemma 7. Since $U^\dagger V$ commutes with X_1 and Z_1 , we have $U^\dagger V = \mathbb{1} \otimes V'$, where $V' \in \mathcal{C}_4^{\otimes n-1}$ acts on qudits $\{2, \dots, n\}$. Assuming that the induction hypothesis holds for $n-1$, V' and hence V can be constructed from S , T , and nearest-neighbor C_Z . \square